I&EC research
Industrial & Engineering Chemistry Research

Article

Cite This: Ind. Eng. Chem. Res. 2019, 58, 6069−6079

pubs.acs.org/IECR

Multilayer Operability Framework for Process Design, Intensification, and Modularization of Nonlinear Energy Systems

Vitor Gazzaneo and Fernando V. Lima*

Department of Chemical and Biomedical Engineering, West Virginia University, Morgantown, West Virginia 26506, United States

ABSTRACT: An optimization-based multilayer operability framework is introduced for the process design of nonlinear energy systems that are challenged by complexity and highly constrained environments. In the first layer of this framework, a mixed-integer linear programming (MILP)-based iterative algorithm considers the minimization of the footprint and the achievement of process intensification targets. Then, in the second layer, an operability analysis is performed to incorporate into the approach key features for optimality and feasibility, accounting for the system operation with changeable input conditions. The outcome of the framework consists of a set of modular designs, considering the aspects of both size and process operability. For this study, the nonlinear system is represented by multiple linearized models, resulting in low computational expense and efficient quantification of operability regions. The developed framework is applied to a membrane reactor for direct methane aromatization conversion to hydrogen and benzene. Subsystems of dimensionalities of 2 × 2 and 3 × 3 (design inputs × outputs) are considered in the first layer to obtain a modular design region. The possible modular designs inside this region are then ranked according to an operability index obtained from an additional 3 × 3 (operational inputs × outputs) mapping. This step analyzes the effect of operational inputs, producing a mapping of total dimensionality of 6 × 3 (inputs × outputs). The application of the developed framework generates two candidate designs for system modularity, the most operable design and the optimal design with respect to process intensification in terms of footprint minimization. The developed framework thus provides guidelines for obtaining modular designs that simultaneously consider process intensification and operability aspects.

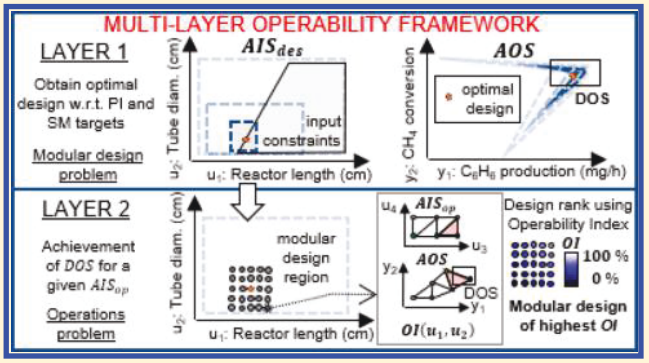

1. INTRODUCTION

Modular systems have been defined as mounted structures composed of steel frames, that is, modules, in which one or multiple unit operations take place.[1] Considering all possible distributions of process operations among these modules, a high degree of process integration can arise when reducing the size of chemical processes for designing small and more efficient integrated units. In particular, process intensification (PI) can provide a set of strategies to design such small and efficient modules.[2]

Once the modules are built, usually offsite, transportation is a key challenge for the feasibility of modular plants. Because there are a few definitions of modular systems in the literature,[1,3] it is important to narrow down such definitions to a tangible characterization that can be directly used for process design. This can be done by adopting a definition of system modularization (SM) associated with the size and weight limitations that are compatible with either maritime, rail, or road transportation.

The way in which the modules will be transported mainly depends on the place and location where the modules are built, typically close to where they will be installed. For example, in the scope of exploitation of natural gas from the Marcellus Shale Formation around the states of West Virginia and Pennsylvania, shipment can be facilitated by road access, resulting in dimension limitations consistent with commercial trucks,[4,5] depicted in Table 1.[6]

Although the physical description of modular systems provides directions for modular process design, other challenges

Table 1. Dimensional Limits for Transportation of Modular Systems by Road

dimension	limit
width	8.5 ft (2.5 m)
height[a]	8.5 ft (2.5 m)
length	53 ft (16.1 m)
volume	3829 ft^3 (108 m^3)
weight[b]	56 000 lb (25 400 kg)

[a]From the flatbed trailer to the top of the load (assuming 5 ft tall flatbed). [b]Excluding the average vehicle weight of ∼32 000 lb (i.e., 80 000 lb total).

Special Issue: Frameworks for Process Intensification and Modularization

Received: November 5, 2018
Revised: March 9, 2019
Accepted: March 14, 2019
Published: March 14, 2019

DOI: 10.1021/acs.iecr.8b05482
Ind. Eng. Chem. Res. 2019, 58, 6069−6079

come from the fact that modular systems still consist of emerging technologies without well-established guidelines and heuristics. Modular systems can be susceptible to unforeseen operational difficulties, which may undermine initially projected optimality and feasibility principles.[7,8]

Recent publications introduced extensions to traditional concepts of process operability to enable PI toward SM.[3,9−12] The employed approaches considered design inputs (physical dimensions) instead of operational variables, which were conventionally chosen as inputs for operability mapping.[8] Nevertheless, once a unique design for SM is obtained, no assessment of process operability quantified, for example, by an operability index (OI) has been reported in the literature, which corresponds to a gap related to the operability evaluation using both design and operational inputs.

Additionally, the modularization of energy systems presents challenges associated with dimensionality, nonlinearities, and a highly constrained environment. To address these challenges, operability calculations employing nonlinear-programming-based (NLP-based) approaches were proposed.[3,9−11] However, with the increase in system dimensionality, drastic growths in computational cost were reported, restricting the operability calculations to multicore systems that include computer tools such as parallel computing.[3]

In addition to the NLP-based approaches, input−output mappings have been used in other methods to quantify operability/flexibility regions for systems of similar complexity. These methods aimed to tackle intrinsic challenges such as space nonconvexities, nonlinearities, and system dimensionality. Some of them are (i) surface-response-based techniques (kriging and surface-response methods[13,14]), (ii) data-driven and design-of-experiments,[13−16] (iii) simplicial approximation,[17] (iv) high-dimensional data-driven model representations,[14,18] (v) multi-parametric approaches,[19,20] and (vi) metamodeling.[21]

In the field of system identification for control applications, plants that presented drastic changes in operating regimes were represented by multiple models to describe the operating regions that represent such regimes. Multiple state-space[22,23] and multiple linear models[24,25] are some of the examples that employed the multimodel concept along the lines of the work presented in this Article.

In this Article, to fill the aforementioned gaps, a computationally efficient multilayer operability framework is developed for the intensification and modularization of nonlinear energy systems. For this study, the original nonlinear models are substituted by multiple linearized models generated using computational geometry techniques. This multimodel representation allows the full employment of linear-programming-based optimization tools and the efficient calculation of the operability regions in high-dimensional spaces. Reductions in computational expense and thus in the necessity of parallel computing are attained as consequences of this model representation.

In the first layer of the developed framework, a mixed-integer linear programming-based (MILP-based) iterative algorithm is introduced with the objective of finding an optimal design point with respect to PI and SM targets (modular design problem). In the second layer, a modular design region is constructed around the obtained optimal point, and the modular designs inside this region are systematically ranked using steady-state operability and the OI (operations problem). An application to a membrane reactor for direct methane aromatization (DMA-MR) conversion to hydrogen and benzene is provided, along with intensified modular designs of best operability.

The following structure is presented as outlined in this Article: In Section 2, the employed operability concepts are explained; in Section 3, details of the multimodel representation are shown; in Section 4, the description of the multilayer operability framework can be found in two subsections, one for each layer of the framework; in Section 5, the DMA-MR application is reported along with results; finally, in Section 6, conclusions about the developed framework are drawn, and directions for future work are presented.

2. PROCESS OPERABILITY CONCEPTS

Set-point operability was generically defined in the literature for the operability analysis of square systems.[26] Considering a system with m inputs, n_x states, and p outputs, the following process model, denoted by M, can describe the system behavior

$$M = \begin{cases} \dot{x} = f(x, u) \\ y = g(x, u) \\ h_1(\dot{x}, x, y, \dot{u}, u) = 0 \\ h_2(\dot{x}, x, y, \dot{u}, u) \geq 0 \end{cases} \tag{1}$$

in which $x \in \mathbb{R}^{n_x}$ are the state variables, $y \in \mathbb{R}^p$ are the outputs, and $u \in \mathbb{R}^m$ are the inputs. The functions f and g are the nonlinear maps, and h_1 and h_2 are the equality and inequality process constraints, respectively. Finally, $\dot{x}$ and $\dot{u}$ represent time derivatives associated with x and u, respectively.

Given the generic process model, M, presented above, one can define two sets that describe the readily accessible information of interest for the operability analysis, as follows:

Available Input Set (AIS): Set of available inputs that may be changed within a certain range according to physical or operating constraints. This set may represent design or operational inputs. Design inputs are associated with available designs (material, dimensions, etc.), whereas operational inputs are the manipulated variables (MVs) subject to control studies. Here this set is mathematically described as follows

$$AIS = \{u | u_i^{\min} \leq u_i \leq u_i^{\max};\ 1 \leq i \leq m\} \tag{2}$$

in which u_i can be either a design variable (for AIS_{des}) or an operational variable (for AIS_{op}).

Desired Output Set (DOS): Set that comprises the desired region of output targets. It may be defined, for example, by process constraints and desired production or efficiency. PI targets can be incorporated here as regions of intensified operation. Mathematically, the *DOS* is defined as

$$DOS = \{y | y_i^{\min} \leq y_i \leq y_i^{\max};\ 1 \leq i \leq p\} \tag{3}$$

Having defined the process model, M, and the two sets above, other regions of interest can be calculated using the direct (M) or inverse model (M^{-1}), and the OI can be evaluated, as outlined below.

Achievable Output Set (AOS): Set of output variables that the system is able to achieve for the considered *AIS*. Under the nominal conditions, this set is defined as

$$AOS = \{y | M(u);\ \forall\ u \in AIS\} \tag{4}$$

in which the AIS can be either AIS_{des} or AIS_{op}.

DOI: 10.1021/acs.iecr.8b05482
Ind. Eng. Chem. Res. 2019, 58, 6069−6079

Desired Input Set (DIS): Set of required inputs that are needed to achieve, if possible, the entire *DOS*. This set can be computed by applying the inverse model to the points in the *DOS*. In the absence of regulatory control, this set is given by

$$DIS = \{u | M^{-1}(y);\ \forall\ y \in DOS\} \tag{5}$$

Because nonlinear systems require a nonlinear model, M, the derivation of M^{-1} may be complex and sometimes not straightforward. One contribution of this work is the numerical computation of M^{-1} employing computational geometry triangulation tools, overcoming the challenges associated with the analytical calculation of M^{-1}. (See Section 3 for details of this calculation.)

With the aforementioned sets, the OI is defined to quantify the achievability of the DOS, as follows

$$OI = \frac{\mu(AOS \cap DOS)}{\mu(DOS)} \tag{6}$$

in which the μ corresponds to a measure of the depicted region. For one dimension, μ is simply a measure of length, for two dimensions, it is a measure of area, for three dimensions, it is measure of volume, and for higher-dimensional cases, it is a measure of hypervolume. For nonsquare systems with more outputs than inputs, the definition of OI would require adaptation to consider the concept of interval operability.[27,28]

3. MULTIMODEL REPRESENTATION

To represent the original nonlinear model, M, using a set of linearized models, a geometric representation using families of paired polytopes is employed. For n-dimensional square systems $(m = p = n)$, each kth pair of polytopes, P_k, links input and output points, as follows

$$P_k = \{P_k^u,\ P_k^y\} \tag{7}$$

$$P_k^u = \{u_{i,jk} \in AIS | 1 \le i \le n;\ 1 \le j \le n+1\} \tag{8}$$

$$P_k^y = \{y_{i,jk} \in AOS | 1 \le i \le n;\ 1 \le j \le n+1\} \tag{9}$$

in which P_k^u is a polytope in the input space, P_k^y is the corresponding polytope in the output space, i is the coordinate representing the dimension of each variable, and j is an assigned number for each vertex. Here the number of vertices, $n + 1$, is used because only simplices are considered for the representation of the polytopes. For example, a 2-D system with three input−output points can be represented by one pair of triangles $(n + 1 = 3$ vertices) with $P_1^u = \left\{\begin{bmatrix}u_{1,11}\\u_{2,11}\end{bmatrix}, \begin{bmatrix}u_{1,21}\\u_{2,21}\end{bmatrix}, \begin{bmatrix}u_{1,31}\\u_{2,31}\end{bmatrix}\right\}$ and $P_1^y = \left\{\begin{bmatrix}y_{1,11}\\y_{2,11}\end{bmatrix}, \begin{bmatrix}y_{1,21}\\y_{2,21}\end{bmatrix}, \begin{bmatrix}y_{1,31}\\y_{2,31}\end{bmatrix}\right\}$. This representation using simplices has the advantage that a simplex is always a convex shape, providing a division of the geometrical nonconvexities into convex sets and facilitating operations such as spatial search and interpolation. Thus for nonconvex input or output spaces, a set of convex simplices would be adopted for their representation.

For a representation with a total number of K polytopes, the *AIS* and *AOS* described in Section 2 can be mathematically represented as follows

$$S = \{1, 2, 3, ..., K\} \tag{10}$$

$$AIS = \{P_k^u | k \in S\} \tag{11}$$

$$AOS = \{P_k^y | k \in S\} \tag{12}$$

in which $S \subseteq \mathbb{N}$ contains the indices for the mappings between input and output simplices, from P_1 to P_K. Figure 1 shows an example of this representation for a generic 2 × 2 system containing six input−output data points.

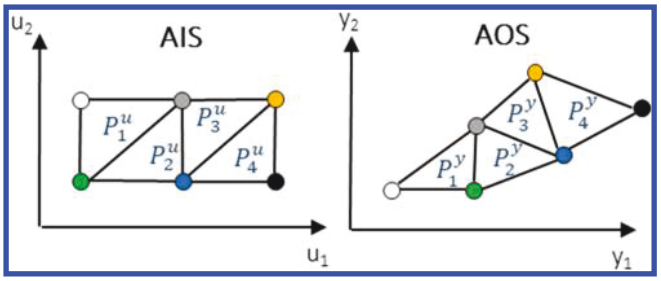

Figure 1. Illustration of the multimodel polytope representation for a 2 × 2 system.

For the case in Figure 1, $S = \{1, 2, 3, 4\}$ with $K = 4$ polytopes that are simplices in two dimensions, that is, triangles. Each pair of triangles links three input−output points, in which the edges correspond to three linear models.

Some advantages when employing the multimodel representation for M are the easy quantification of the OI and the straightforward model inversion M^{-1} using computational geometry tools. In particular, the calculations of M^{-1} are performed for a region of the *AOS* by selecting the output polytopes inside such region and then verifying which are the corresponding paired polytopes in the *AIS*. Still using the example above, suppose one verifies that $DOS \cap AOS = \{P_3^y, P_4^y\}$; therefore, $M^{-1}[DOS \cap AOS] = \{P_3^u, P_4^u\}$, associated with two triangles in the input space. If needed, interpolations can be applied to obtain M^{-1} in terms of the points inside the triangles. Such multimodel representation can be produced from space discretization techniques such as Delaunay triangulation, described in Section 4.

4. MULTILAYER OPERABILITY FRAMEWORK

The developed multilayer operability framework tackles both the modular design and the operational problems. The framework is developed with the assumption that the nonlinear system in focus is operating away from singularities in the output space. In each layer, the original nonlinear model is substituted by a multimodel representation according to the adopted subsystem and definition of operability spaces, as described above.

On the basis of this new system representation, the proposed multilayer framework is composed of two layers. In the first layer, an iterative MILP formulation is introduced for the calculation of the optimal design with respect to PI and SM targets. Then, an operability analysis using the OI is performed considering a modular design region around where the optimal design was obtained. Each of these layers is described below in the following subsections.

4.1. MILP-Based Iterative Algorithm. For the first layer, the considered AIS is exclusively associated with design variables, producing an AIS_{des}−*AOS* mapping. To eliminate the need for extensive simulations, instead of generating a detailed multimodel representation for the entire AIS_{des} and AOS,[12] an iterative algorithm is developed so that the number of models locally increases as the program approaches the optimal

DOI: 10.1021/acs.iecr.8b05482
Ind. Eng. Chem. Res. 2019, 58, 6069−6079

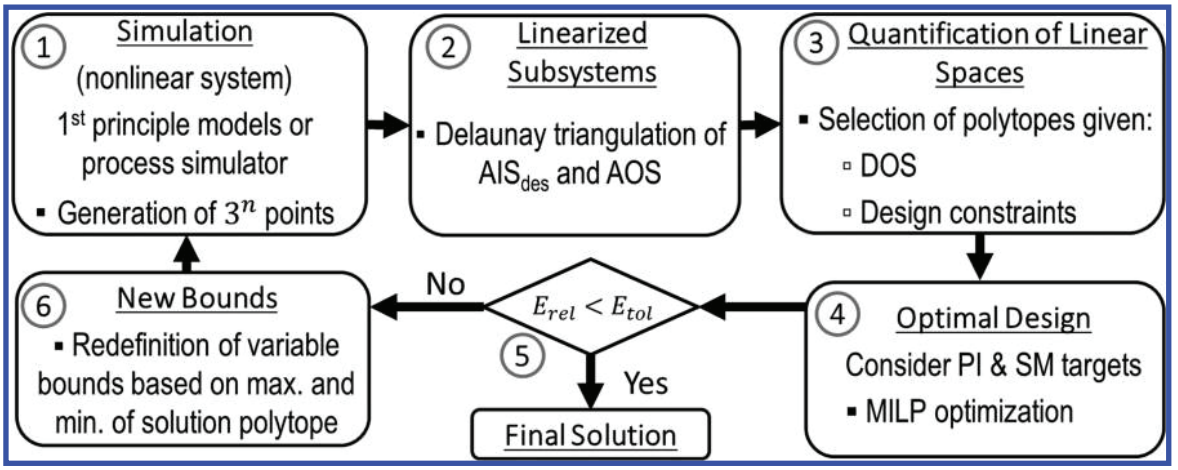

Figure 2. Steps of the MILP-based iterative approach (Layer 1).

design region. Starting with the entire AIS_{des} set, in each iteration, a solution is generated, so that the input space is gradually narrowed around the optimal solution. When there is no change in the solution from one iteration to the next, the algorithm achieves convergence, and the optimal design region is obtained. Computational geometry triangulation tools are employed for the calculation of intersections involving the set of obtained geometrical entities that represent the linearized models.[29,30] The algorithm is developed to accommodate a generic number of dimensions. Figure 2 shows a schematic representation of the developed algorithm with all of the employed steps.

Each of the enumerated steps in Figure 2 is briefly discussed below.

(1) *Simulation*: According to the energy system application of interest, 3^n data points are generated using either first-principle models or a process simulator, in which n ($n = m = p$) is the dimensionality of the analyzed square system (2-D, 3-D, etc.). This number of data points is chosen to obtain a relatively low number of function evaluations of the process model M in each iteration and thus maintain a low computational expense. Alternatively, a less coarse initial grid could be adopted in the initial iterations for a more detailed representation of the nonlinear system with the expense of a higher computational time. Because the available inputs are known, the input set is evenly divided into a grid, and the corresponding output points can be obtained through simulation. This uniform grid division is adopted here because it provides a lower computational time for the task of finding approximated optimal points in step 4. A nonuniform division of the grid would be recommended for the task of further characterizing the representation of $AOS \cap DOS$. The outcome of this step is a set of input−output data points.

(2) *Linearized Subsystems*: Using the obtained input−output data points, the spatial discretization technique of Delaunay triangulation is applied to build the multimodel representation. This triangulation is performed using input points. The connections among these input points is then obtained and applied to calculate the corresponding polytopes in the output space. This technique generates a set of K paired polytopes that is indexed by $S = \{1, 2, ..., K\}$. Each pair of polytopes, P_k, represents a set of linear models from the input to the output space. The set S is used to indicate all of the K paired polytopes, that is, $\{P_k | k \in S\}$.

(3) *Quantification of Linear Spaces*: The obtained polytopes are analyzed according to achievability of the DOS and also input constraints. For achievability, the intersection $DOS \cap AOS$ provides the pairs of polytopes that guarantee the achievability of the DOS. At the same time, the intersection between AIS_{des} and input constraints is considered for the selection of pairs of polytopes that satisfy such input constraints. The outcome of this step is a set $S' \subseteq S$ of K' paired polytopes that satisfy the criteria for the inputs and outputs.

(4) *Optimal Design*: To obtain an optimal design point, an MILP minimization problem is formulated for the selection of the pair of polytopes from S' that gives the optimal input−output coordinates considering PI, SM, and process constraints. Weights associated with vertices of the polytopes and barycentric interpolations allow this optimal solution to be inside one of the considered polytopes. In addition to the weights, a binary variable is assigned to each pair of polytopes so that the MILP solver selects only one pair as a solution. The MILP-minimization problem can be mathematically represented as follows

$$\phi = \underset{u, b_k}{\text{minimize}} \ (\textit{linearized footprint})$$

Subject to:

$$u \in AIS_{des},\ y \in DOS$$

$$b_k \in \{0, 1\}^{K'}$$

$$\sum b_k = 1$$

$$\textit{PI and SM targets}$$

$$\textit{Process constraints}$$

in which b_k is the binary variable assigned to each pair of polytopes, P_k, from $\{P_k | k \in S'\}$. The MILP-minimization problem results in a selected pair of polytopes, P_{sol}, in which the obtained optimal solution is inside. The optimal solution corresponds to one input−output point calculated from barycentric interpolations using the vertices of P_{sol}. This point is, therefore, associated with an input $u \in AIS_{des}$, mapped to some $y \in AOS$. The MATLAB subroutine intlinprog is used here to solve the formulated problem with tolerances for both integers and constraints of 0.001. Additional details of this formulation can be found along with its application in Section 5.2.

(5) *Stopping Criteria*: Using the solution for the optimal design of the current iteration and the solution of the previous

DOI: 10.1021/acs.iecr.8b05482
Ind. Eng. Chem. Res. 2019, 58, 6069−6079

iteration, the relative difference between solutions is calculated, E_{rel}. If this difference is smaller than a predefined threshold or tolerance, E_{tol}, then the algorithm converges, and the final solution is obtained (*Final Solution*). Otherwise, new variable bounds are redefined based on the polytope of the current solution (step 6).

(6) *New Bounds*: If the algorithm has not converged, then new input bounds are chosen based on the selected pair of polytopes from step 4, P_{sol}. These bounds are described by the set $\{u_{i,P_{sol}}^{min} \le u_i \le u_{i,P_{sol}}^{max} | 1 \le i \le n\}$, in which $u_{i,P_{sol}}^{min}$ and $u_{i,P_{sol}}^{max}$ are the minimum and maximum values that characterize the polytope of the solution in the inputs. For each dimension i (up to n), the new minimum and maximum bounds are calculated as follows

$$u_{i,P_{sol}}^{min} = \min(\{u_{i,jP_{sol}} | 1 \le j \le n+1\}) \quad (13)$$

$$u_{i,P_{sol}}^{max} = \max(\{u_{i,jP_{sol}} | 1 \le j \le n+1\}) \quad (14)$$

in which j refers to each vertex of the polytope of the solution P_{sol}. As explained in Section 3, P_{sol} has $n+1$ vertices because it is a simplex shape. For example, in 2-D, P_{sol} would be a triangle and the bounds would be given by a parallelogram around P_{sol}; in 3-D, it would be a tetrahedral and the bounds, a parallelepiped; and so on. Once the new bounds are defined, the algorithm goes back to step 1 for the next iteration.

4.2. Operability Analysis around Optimal Design. In the second layer, using the obtained optimal design point (final solution above) that accounts for PI and SM targets, a box of modular designs is built around this point, considering feasible construction values. For different designs inside the box, the output achievability is analyzed by employing an AIS_{op}−AOS operational mapping. The developed approach is restricted to set point operability, and it is applied here to square systems. For this analysis, the AIS_{op} is strictly composed of MVs that would be used for the control.

Each operational mapping relies on a multimodel representation that comes from the application of computational geometry/triangulation tools described in Section 4.1. The operability analysis employs the operational mappings to determine values of the OI so that the designs of the modular region are ranked. Figure 3 contains an illustration of this layer.

The values of OI above quantify the achievability of system objectives and are computed by measuring the number of subregions of the *DOS* that can be achieved given the considered AIS_{op}. A subregion of the *DOS* is assumed to be achievable when it contains at least one point of the *AOS* in its interior. The bigger the value of the OI, the higher the achievability of the *DOS*.

The design of the highest OI is selected, and a final study contrasting the selected point and the previously obtained optimal design can then be performed. This comparison includes the OI and the region of the AIS_{op} that is needed for achievability of the *DOS*.

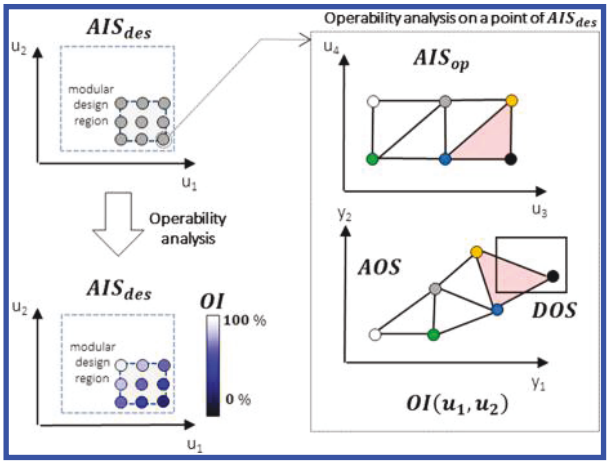

Figure 3. Ranking modular designs using the OI (Layer 2).

5. DMA-MR APPLICATION

The DMA-MR for conversion to hydrogen and benzene is selected for the application of the multilayer operability framework. Figure 4 shows a schematic representation of the DMA-MR with its respective reactions involved.[11]

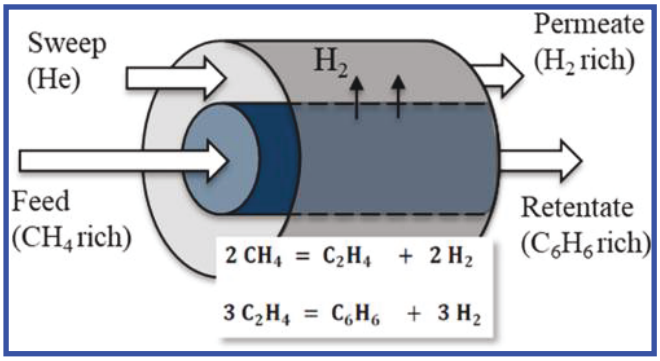

Figure 4. DMA-MR schematic with reactions involved.

Reaction and separation through the membrane are combined in a way such that the selective H_2 removal shifts the reaction toward the products. This feature increases the overall system efficiency, reducing the size of the chemical process and characterizing the DMA-MR as a candidate for PI with SM strategies. Moreover, this system consists of a promising application for modular natural gas utilization, allowing the modular production of a fuel (H_2) and a value-added chemical (C_6H_6). The ultimate goal of producing an intensified modular system that maximizes methane conversion to H_2 and C_6H_6 is considered in all of the cases addressed below.

In this section, first, some aspects of the employed DMA-MR model are described. Then, the multilayer operability framework is applied considering the MILP-based iterative algorithm application to 2 × 2 and 3 × 3 (AIS_{des} × AOS) DMA-MR subsystems, followed by the operability analysis for the 3 × 3 subsystem (AIS_{op} × AOS).

5.1. DMA-MR Model and Simulation. The DMA-MR is modeled using a set of ordinary differential equations (ODEs) built employing steady-state molar balances on the tube and shell sides with respect to the reactor axial coordinate (see the model details including the system of equations in ref 11). For this application, the nominal values for the parameters depicted in Table 2 are used, unless otherwise indicated.

The parameter η in Table 2 is the effectiveness factor for the catalyst that is explicitly included in the model found in the literature[11] to account for the effect of catalyst effectiveness and bed void. This factor consists of a multiplier for all reaction rates present in the ODE set, resulting in $r_1^{actual} = \eta r_1$ and $r_2^{actual} = \eta r_2$. Also, for this study, the volumetric flow rates are converted to molar flow rates assuming ideal gas behavior.

For the generation of the input−output operability mappings present in both tasks of the multilayer operability framework,

DOI: 10.1021/acs.iecr.8b05482
Ind. Eng. Chem. Res. 2019, 58, 6069−6079

Table 2. Overall Parameter Values Considered for the DMA-MR Simulations

parameter	nominal value [unit]
rate constant of direct reaction 1, k_1	0.04 [s^{-1}]
rate constant of inverse reaction 1, k_1'	6.40 × 10^6 [cm^3 s^{-1} mol^{-1}]
rate constant of direct reaction 2, k_2	4.20 [s^{-1}]
rate constant of inverse reaction 2, k_2'	56.38 [cm^3 s^{-1} mol^{-1}]
membrane permeance, Q	3.6 × 10^{-6} [mol h^{-1} cm^{-2} $atm^{-1/4}$]
membrane selectivity, $\alpha_{H_2,all} = \alpha$	1000 [−]
shell diameter, d_s	3 [cm]
tube diameter, d_t	0.5 [cm]
reactor length, L	10 [cm]
tube and shell pressure, P_s and P_t	101 325 [Pa]
temperature, T	1173.15 [K]
volumetric flow of methane inlet, v_{CH_4}	8 [cm^3/min]
volumetric flow of sweep gas inlet, v_{He}	10 [cm^3/min]
effectiveness factor for catalyst, η	0.45 [−]

data points are obtained from simulations performed in MATLAB using the ODE solver "ode15s", recommended for stiff ODEs. The step size for the independent variable reactor length is either 0.01 cm or is automatically adjusted if it is within the investigated range in the optimization.

5.2. MILP-Based Iterative Algorithm Application. The MILP-based iterative algorithm is applied for DMA-MR subsystems of different dimensionalities. The goal of this layer is to find the minimum reactor size and thus achieve SM for given PI targets. The outcome is a modular system calculated for the nominal operation described in Table 2, that is, nominal pressure, temperature, and inlet flows.

5.2.1. Optimal Design for the 2 × 2 DMA-MR Subsystem. For the 2 × 2 case, the AIS_{des} is built considering input ranges from 10 to 100 cm for reactor length and 0.5 to 2.0 cm for tube diameter, associated with variables u_1 and u_2, respectively. The *AOS* is characterized by the outputs of benzene production in mg/h and methane conversion, associated with the variables y_1 and y_2, respectively. For the DMA-MR system, previous work[11] indicates an expected *DOS* given by ranges of 20 to 25 mg/h for benzene production and 0.35 to 0.45 for methane conversion.

To achieve SM, the main objective of this operability layer is to find the optimal design with respect to footprint (size) reduction while respecting PI targets and process constraints. As an intensification target, a minimal benzene production of 20 mg/h is considered, whereas the ratio using the length of reactor (L) and tube diameter (D) of $L/D \geq 30$ is specified as a constraint for plug-flow reactor operation.[31]

The application of each of the steps of the iterative algorithm introduced in Section 4.1 is explained below.

(1) *Simulation*: Here in the first iteration, the input bounds $u_1 = [10\ 100]$ and $u_2 = [0.5\ 2.0]$ are evenly divided into $3^2 = 9$ input points. The output points are obtained through the simulation of the nonlinear system using the process model M. In Figure 5a, it is possible to see the formed grid for selected iterations. In Figure 6a, the obtained output for each iteration is depicted.

(2) *Linearized Subsystems*: The obtained input−output points are used as inputs for this step, generating the multimodel representation. Figures 5a and 6a depict the sets of connected triangles for each iteration, indicated by $S = \{1, 2, ..., 8\}$.

(3) *Quantification of Linear Spaces*: Using the obtained multimodel representation from step 2, the paired triangles that satisfy both input ($L/D \geq 30$) and output (DOS) constraints are selected, generating a subset $S' \subseteq S$. Figures 5b and 6b show the

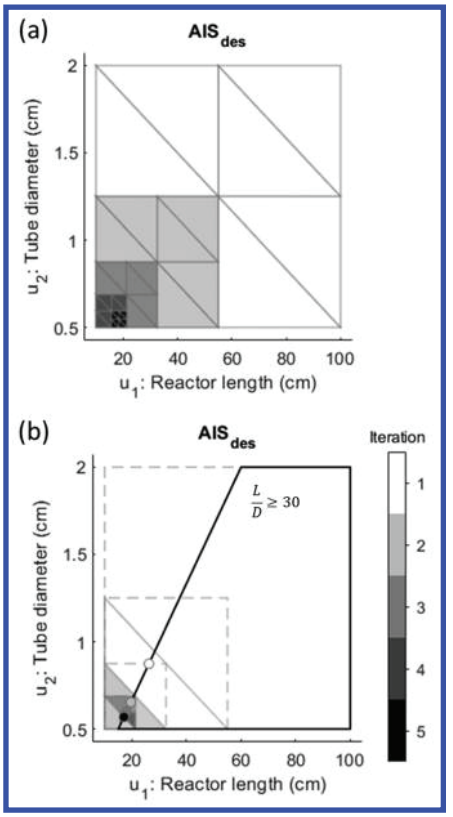

Figure 5. 2-D case: (a) input variable bounds and triangulation and (b) selection of triangles and optimal solution points for each iteration.

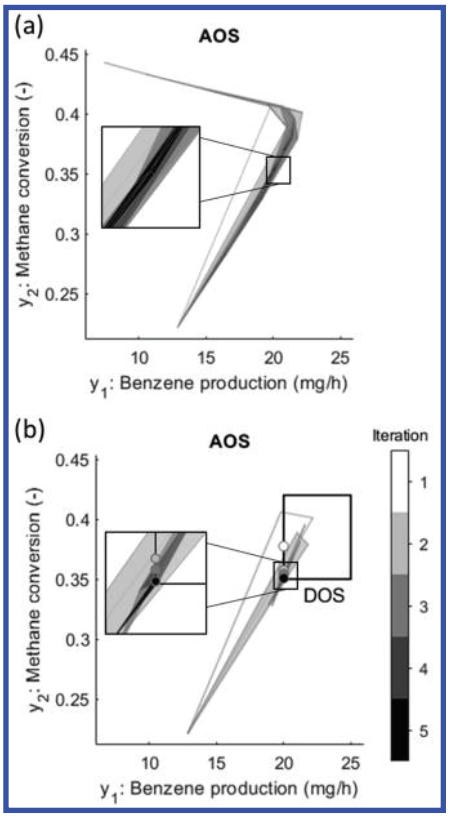

Figure 6. 2-D case: (a) output mapping and (b) selection of triangles and optimal solution points for each iteration.

DOI: 10.1021/acs.iecr.8b05482
Ind. Eng. Chem. Res. 2019, 58, 6069−6079

regions associated with the input and output constraints, respectively.

(4) *Optimal Design*: Using the paired triangles given by S', the MILP formulation is described as

$$\phi = \underset{w_{jk}, b_k}{\text{minimize}} \ (h(u_1, u_2))$$

Subject to:

$$u_1/u_2 \geq 30$$

$$y_1 \geq 20$$

$$0 \leq w_{jk} \leq 1, \ k \in S', \ j \in \{1, 2, 3\}$$

$$u_i = \sum_{k=1}^{K'} \left(\sum_{j=1}^{3} u_{i,jk} \cdot w_{jk} \right), \ i \in \{1, 2\}$$

$$y_i = \sum_{k=1}^{K'} \left(\sum_{j=1}^{3} y_{i,jk} \cdot w_{jk} \right), \ i \in \{1, 2\}$$

$$\sum_{j=1}^{3} w_{jk} = b_k, \ k \in S'$$

$$b_k \in \{0, 1\}, \ k \in S'$$

$$\sum_{k=1}^{K'} b_k = 1$$

in which b_k is the binary variable assigned to each pair of triangles, P_k, $k \in S'$; w_{jk} is the weight of a vertex, j, in a pair of triangles, k; and $u_{i,jk}$ and $y_{i,jk}$ are the input−output data points of a pair of triangles, P_k. The footprint, initially given by the sum of total membrane area and reactor volume is approximated here by a linearization around the nominal reactor length and tube diameter as follows

$$h(u_1, u_2) = (D_0 + 0.25D_0^2)u_1 + (L_0 + 0.5L_0D_0)u_2$$
$$= 0.5625u_1 + 12.5u_2 \quad (15)$$

in which L_0 = 10 cm and D_0 = 0.5 cm are the nominal values of reactor length and tube diameter, respectively.

Figures 5b and 6b show the selection of a triangle in each iteration, for inputs and outputs, respectively, as well as the calculation of the optimal points (plotted inside the figures).

(5) *Stopping Criteria*: A tolerance error of 1% with respect to each variable for both input and output coordinates is considered for convergence to the optimal solution.

(6) *New Bounds*: Smaller regions of the *AIS* are considered as the algorithm approaches convergence. Figure 5a shows these regions being reduced until convergence is achieved.

For the 2 × 2 subsystem, the algorithm converges to an optimal solution in five iterations, and the result is a DMA-MR with reactor length of 17.05 cm and tube diameter of 0.57 cm that corresponds to a benzene production of 20 mg/h and methane conversion of 0.35. The total computational time of the algorithm is of 6 s.

5.2.2. Optimal Design for the 3 × 3 DMA-MR Subsystem. For this case, the dimensionality of the 2 × 2 subsystem is augmented by adding the input variable of membrane selectivity to the AIS_{des} and the output variable of hydrogen production to the *AOS*. It is assumed here that the membrane selectivity could be improved in the lab if needed to achieve the desired process specifications.[32] The initial range for membrane selectivity considering lab expectation values is 1×10^2 to 1×10^5.[10] Prescreening of the solution space is performed to eliminate potential singularities in the output space, and this range is modified here to 3×10^2 to 1×10^5. Membrane selectivity values below 3×10^2 provide a result with very low to no methane conversion.

The benzene production and methane conversion ranges in *DOS* are kept the same, whereas the hydrogen production has its range set from 3 to 6 mg/h.

The same SM and PI targets from the 2-D case are maintained as well as the plug-flow constraint. The application of each of the steps of the iterative algorithm is performed considering small changes from the previous case, as described below. For illustration purposes, the presentation of the algorithm is simplified, containing only three iterations, the first, one intermediate (fourth), and the last iteration (eighth).

(1) *Simulation*: Now, in the first iteration, with the addition of the membrane selectivity variable bounded as $u_3 = [3 \times 10^2 \ 1 \times 10^5]$, $3^3 = 27$ input−output points are obtained through simulation. In Figures 7 and 9, it is possible to see the formed grid for each iteration.

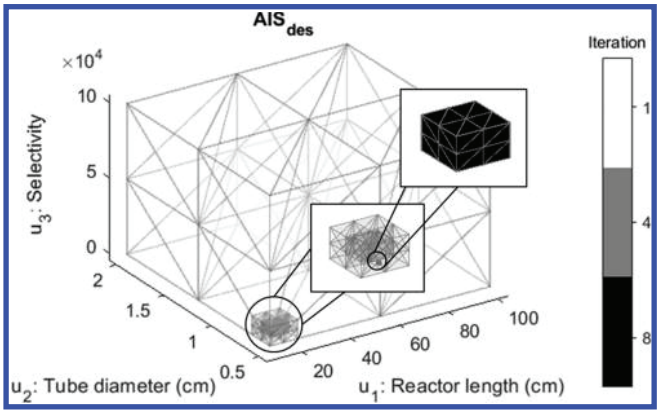

Figure 7. 3-D case: Input variable bounds and 3-D triangulations.

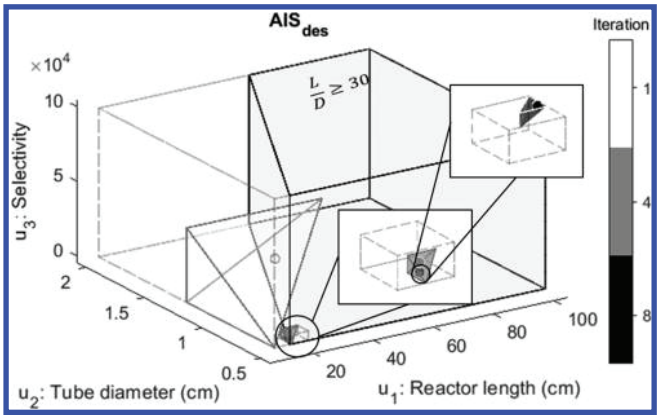

Figure 8. 3-D case: Selection of tetrahedra and optimal solution points.

(2) *Linearized Subsystems*: Using the obtained grid, the Delaunay triangulation is performed, and the set $S = \{1, 2, ..., 48\}$ indicates the obtained pairs of tetrahedra, depicted in Figures 7 and 9.

(3) *Quantification of Linear Spaces*: The obtained multimodel representation in step 2 is used here. Similarly to the 2-D case, a subset $S' \subseteq S$ indicates the paired tetrahedra that satisfy both

DOI: 10.1021/acs.iecr.8b05482
Ind. Eng. Chem. Res. 2019, 58, 6069−6079

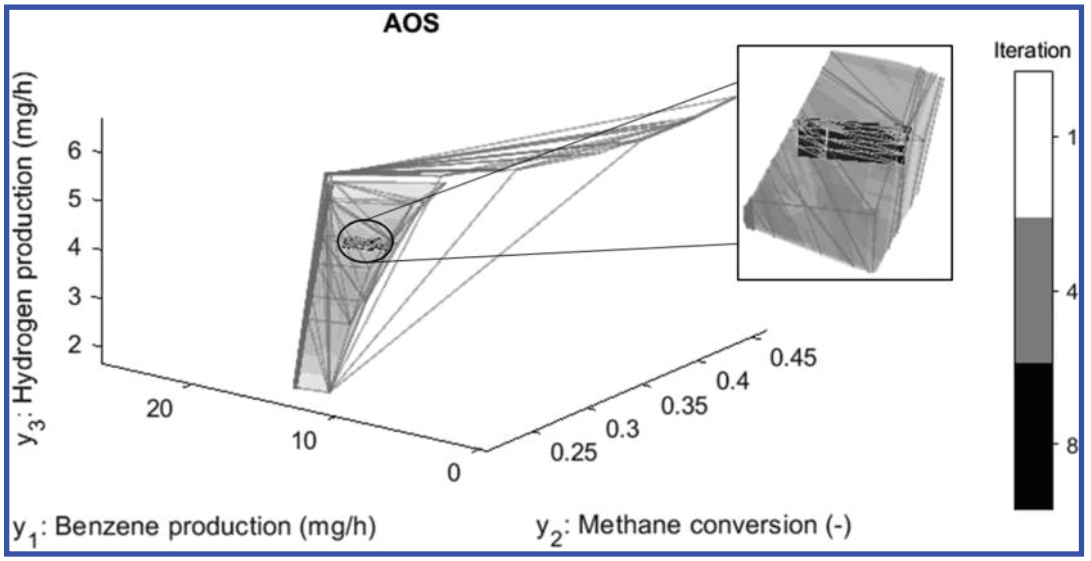

Figure 9. 3-D case: Output mapping.

input and output constraints. The input and output regions can be found in Figures 8 and 10, respectively.

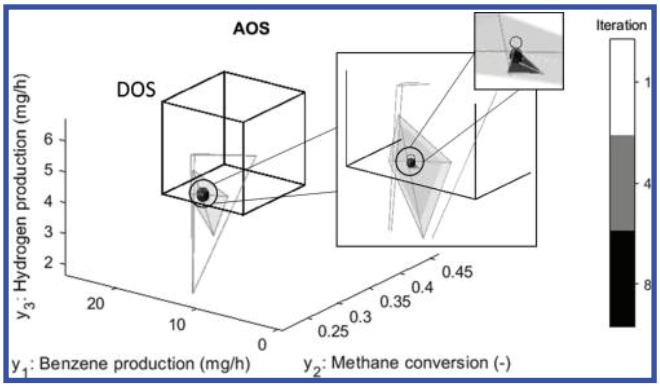

Figure 10. 3-D case: Selection of tetrahedra and optimal solution points.

(4) *Optimal Design*: Because the PI and SM targets as well as constraints are the same as in the previous case, the MILP formulation is changed by only increasing its dimensionality from 2-D to 3-D as follows

$$\phi = \underset{w_{jk}, b_k}{\text{minimize}} \; (h(u_1, u_2))$$

Subject to:

$$u_1/u_2 \geq 30$$

$$y_1 \geq 20$$

$$0 \leq w_{jk} \leq 1,\ k \in S',\ j \in \{1, 2, 3, 4\}$$

$$u_i = \sum_{k=1}^{K'} \left(\sum_{j=1}^{4} u_{i,jk} \cdot w_{jk} \right),\ i \in \{1, 2, 3\}$$

$$y_i = \sum_{k=1}^{K'} \left(\sum_{j=1}^{4} y_{i,jk} \cdot w_{jk} \right),\ i \in \{1, 2, 3\}$$

$$\sum_{j=1}^{4} w_{jk} = S_k,\ k \in S'$$

$$b_k \in \{0, 1\},\ k \in S'$$

$$\sum_{k=1}^{K'} b_k = 1$$

in which y_3 is the hydrogen production in mg/h and the other variables follow the same notation adopted in the previous case.

Figures 8 and 10 show the selection of a tetrahedron in the first, fourth, and eighth iterations as well as the calculation of the optimal points (plotted inside the figure).

(5) *Stopping Criteria*: As in the previous case, a tolerance error of 1% with respect to each variable is considered for convergence.

(6) *New Bounds*: Similarly to the 2-D case, Figure 7 shows how the input bounds are reduced until convergence is obtained.

The algorithm converges to a solution in eight iterations, and the result is a DMA-MR with a reactor length of 16.99 cm, tube diameter of 0.57 cm, and membrane selectivity of 1037 that corresponds to a benzene production of 20 mg/h, methane

Table 3. MILP-Based Iterative Approach Results for the DMA-MR

dim.	reactor length (cm)	tube diameter (cm)	membrane selectivity	C_6H_6 prod. (mg/h)	CH_4 conv. (−)	H_2 prod. (mg/h)	CPU time (s)
2 × 2	17.05	0.57	1000	20	0.35	3.31	6
3 × 3	16.99	0.57	1037	20	0.35	3.29	34

DOI: 10.1021/acs.iecr.8b05482
Ind. Eng. Chem. Res. 2019, 58, 6069−6079

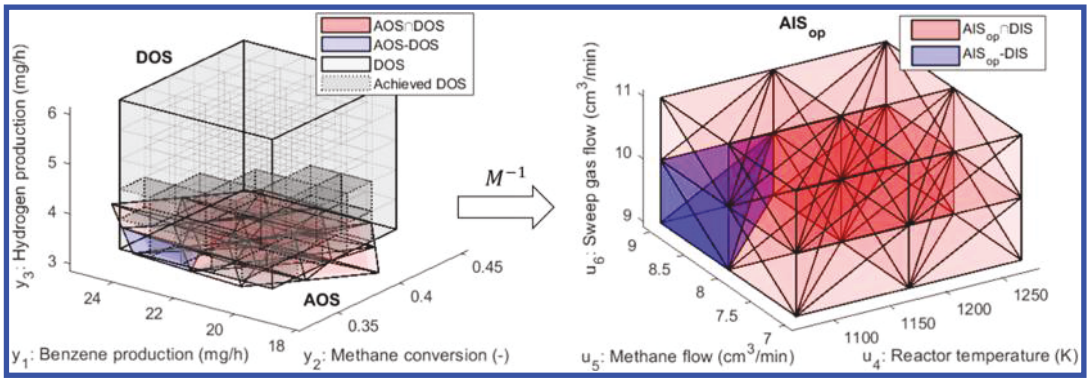

Figure 11. OI and model inversion for design of highest OI.

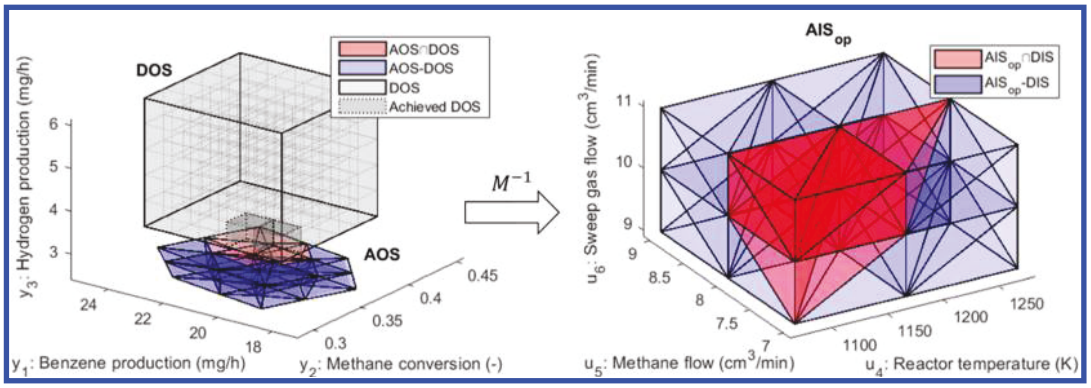

Figure 12. OI and model inversion for previously obtained optimal design.

conversion of 0.35, and hydrogen production of 3.29 mg/h. The total computational time for the algorithm convergence is of 34 s.

5.2.3. Computational Results. The results for the application of the MILP-based iterative approach for DMA-MR subsystems of dimensionalities 2 × 2 and 3 × 3 are compiled in Table 3, which contains the obtained design points and the CPU times.

When contrasting the 2 × 2 and 3 × 3 obtained designs, it is clear that the two designs are practically the same. In this case, the addition of two new input−output variables does not significantly change the results because the 2 × 2 DMA-MR subsystem employs a fixed value of membrane selectivity (1000) that is already close to the obtained optimal design for the 3 × 3 subsystem (1037).

By analyzing the CPU times for both cases, although some increase in computational time is presented when going from 2-D to 3-D, the total computational time is still on the order of seconds. For the NLP-based approaches in the literature,[9] to obtain the optimal solution using a single processor, typical CPU times on the order of minutes for the 2-D case and hours for the 3-D case are reported, showing that the higher the dimensionality of the system, the bigger the advantage of the developed iterative algorithm over NLP-based approaches. The relatively low increase in CPU time thus indicates the promising capabilities of the developed algorithm for expansion to high-dimensional cases.

5.3. Operability Analysis around Optimal Design (for 3 × 3 Subsystem). Considering the 3 × 3 DMA-MR subsystem above and the obtained optimal design, a modular box with values that would be more reasonable for construction is built using reactor lengths from 16 to 18 cm, tube diameters from 0.5 to 0.6 cm, and membrane selectivities from 500 to 1500. The steps of 0.2 cm, 0.01 cm, and 100 are applied to each variable, respectively, to obtain rounded values that would be suitable for manufacturing the possible modular designs. The result is a total of 11^3 = 1331 possible designs that cover approximately ±5% around the obtained optimal design, representing a modular design region constructed based on the outcome of the first layer of the framework.

Then, the *AIS* that was originally composed of $\{u_1, u_2, u_3 \in AIS_{des}\}$ is augmented with the inclusion of operational inputs, namely, $\{u_4, u_5, u_6 \in AIS_{op}\}$. To build the AIS_{op}, variations within ranges of about ±10% from the nominal values (in Table 2) are applied to each of the variables of reactor temperature (u_4), sweep gas inlet flow (u_5), and methane inlet flow (u_6). The final calculated ranges are given by $1073.15 \le u_4 \le 1275.15$ [K], $7 \le u_5 \le 9$ [cm^3/h], and $9 \le u_6 \le 11$ [cm^3/h]. The design and operational subsystems characterize two square systems associated with the same *AOS*, and thus the *AIS* is described by $AIS = AIS_{des} \times AIS_{op}$, $AIS \subseteq \mathbb{R}^6$, associated with an overall *AIS* × *AOS* mapping of dimensionality 6 × 3.

As shown in the framework schematic in Figure 3, for each of the 1331 possible design points in the AIS_{des}, the design is fixed, and an AIS_{op}−*AOS* operability analysis is performed, keeping the same DOS listed in the 3 × 3 case above. For each AIS_{op}−*AOS* mapping, a multimodel representation is obtained by applying the same methodology as in Section 5.2.2 (steps 1 and 2). Similarly, the obtained mapping is given by a set of 48 paired tetrahedra, that is, $\{P_k | k \in S\}$ and $S = \{1, 2, ..., 48\}$. This multimodel representation can be seen in Figures 11 and 12.

To quantify the achievability of each design by the OI, the *DOS* is evenly divided into 125 subregions, represented by 125 parallelepipeds. The number 5^3 = 125 is chosen to define parallelepipeds in which the sides have lengths of 1 mg/h for benzene production, 0.02 for methane conversion, and 0.6 mg/h

DOI: 10.1021/acs.iecr.8b05482
Ind. Eng. Chem. Res. 2019, 58, 6069−6079

for hydrogen production. The OI corresponds to the percentage of these 125 subregions that a considered design can achieve, given the described AIS_{op}. Figures 11 and 12 contain examples of the divided *DOS* and calculations of the OI. In Figure 11, 22 of 125 subregions of the DOS are achieved, corresponding to an OI value of 17.6%, whereas in Figure 12, only two of these subregions are achieved, corresponding to an OI value of 1.6%.

After the described operability analysis is completed for all points of the modular design region, the values of OI are used to rank the considered designs. From this ranking, the design of maximum OI is then selected, consisting of a design with reactor length of 18 cm, tube diameter of 0.6 cm, and membrane selectivity of 1500. Figure 13 shows the rankings using values of

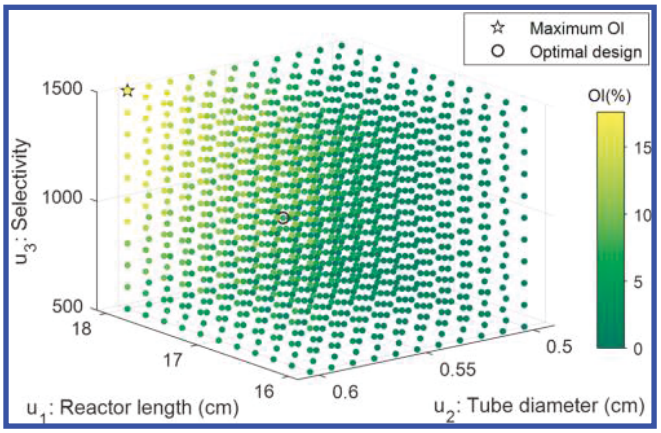

Figure 13. Achievability analysis using OI of designs around the optimal design.

OI, the selected design of maximum OI, and the previously obtained optimal design, rounded to a reactor length of 17 cm, tube diameter of 0.57 cm, and membrane selectivity of 1000.

Figures 11 and 12 represent the individual $AIS_{op}-AOS$ operability analysis of the design of maximum OI (17.6%) and the previously obtained optimal design (with OI of 1.6%), respectively. For both cases, the model inversion $M^{-1}[DOS \cap AOS]$ is performed to produce additional comparative information. The resulting paired polytopes from this operation are identified in red.

When contrasted with the design of maximum OI, the optimal design presents lower values for reactor length, tube diameter, and membrane selectivity. However, the number of *DOS* achieved subregions is 2, which is a relatively low achievability when compared with the best OI case, with 22 achieved subregions. Also, from the 48 tetrahedra that represent the available operational inputs of the AIS_{op}, the highest OI design covers 46 tetrahedra, whereas the optimal design covers only 9, indicating a better exploitation of the AIS_{op} for the achievement of the *DOS* in the highest OI case.

The presented result can be attributed to the fact that the iterative algorithm computes an optimal point of AIS_{des} for a fixed operating condition (a point of the AIS_{op}). The goal of the algorithm is to solely minimize the objective function, given by the linearized footprint, without considering process operation. The operability analysis presented above indicates that slightly bigger reactors are more operable with respect to the considered AIS_{op} and *DOS*. Moreover, the trends in Figure 13 indicate that because higher values of OI are obtained for larger reactors, the objectives of minimizing size and maximizing OI are conflicting in this case.

Taking the design of highest OI as the most operable design, an estimation of a multitubular reactor is made. Assuming a shell of diameter of 50 cm, length of 18 cm, and approximate distance of 0.7 cm among adjacent tubes, a total amount of 1111 tubes can be placed inside the shell. The obtained multitubular modular design can convert 113 ft^3 of methane to 574 g of benzene and 94 g of hydrogen per day.

A commercial truck, as specified in Table 1, could transport a maximum number of modules of ~2225. In a hypothetical scenario in which all of these modules are installed, a total consumption of ~252 Mcf/day of methane would take place. A well in the Marcellus Shale Formation can produce from 500 Mcf/day to 12 MMcf/day of natural gas depending on the well maturity.[33,34] Thus, 2 to 24 trucks, if used to transport the modular units, could allow the onsite utilization of the natural gas installed by a typical well from this region.

6. CONCLUSIONS

A multimodel operability framework was presented for the design of emerging technologies characterized by SM and PI. This framework is flexible and could also be extended to attain other goals such as cost, environmental targets, capacity, purity, and so on. The representation of the nonlinear system by linearized models, geometrically represented by polytopes, was systematically applied for the calculation of an optimal design and operability assessment to ensure future feasibility and optimality.

The developed framework shows unique features for tackling energy system applications whose design is challenged by dimensionality, nonlinearities, and highly constrained environments. The linear approximation minimizes expensive computing, which would be of special importance in high-dimensional cases. The utilization of the OI as a measure for ranking competing designs has not been explored in SM and PI literature before this study. The obtained results showed that the calculation of an optimal modular design considering a fixed nominal operation does not necessarily ensure the best system operability.

A comparison between the distinct tasks of minimizing the footprint to achieve SM while respecting PI targets and maximizing the process operability represented by the OI showed that these two objectives might be conflicting. Future work considering the development of a multiobjective optimization-based operability framework will be pursued to produce modular systems with maximum operating capabilities. The augmentation of system dimensionality is an object of current research work, and it will also be incorporated into newly developed studies.

AUTHOR INFORMATION

Corresponding Author

*E-mail: fernando.lima@mail.wvu.edu.

ORCID

Fernando V. Lima: 0000-0003-4306-1826

Notes

The authors declare no competing financial interest.

ACKNOWLEDGMENTS

We gratefully acknowledge the Donors of the American Chemical Society Petroleum Research Fund and the National Science Foundation CAREER Award 1653098 for partial support of this research.

DOI: 10.1021/acs.iecr.8b05482
Ind. Eng. Chem. Res. 2019, 58, 6069−6079

REFERENCES

(1) Roy, S. Consider Modular Plant Design. *Chem. Eng. Prog.* **2017**, *113* (5), 28−31.
(2) Baldea, M.; Edgar, T. F.; Stanley, B. L.; Kiss, A. A. Modular Manufacturing Processes: Status, Challenges, and Opportunities. *AIChE J.* **2017**, *63* (10), 4262−4272.
(3) Carrasco, J. C.; Lima, F. V. Bilevel and Parallel Programing-Based Operability Approaches for Process Intensification and Modularity. *AIChE J.* **2018**, *64* (8), 3042−3054.
(4) Heavy Haul Trucking. Tractor Trailer Dimensions. http://www.heavyhaul.net/tractor-trailer-dimensions/ (accessed May 10, 2018).
(5) Road Weight and Size Limitations. http://www.cargoagents.net/resources/stateroadweightsizelimitations.htm (accessed Feb 28, 2019).
(6) Haque, A.; et al. *CHE 455: Senior Design Report*; West Virginia University, 2018.
(7) Swaney, R. E.; Grossmann, I. E. An Index for Operational Flexibility in Chemical Process Design. Part I: Formulation and Theory. *AIChE J.* **1985**, *31* (4), 621−630.
(8) Vinson, D. R.; Georgakis, C. New Measure of Process Output Controllability. *J. Process Control* **2000**, *10* (2−3), 185−194.
(9) Carrasco, J. C.; Lima, F. V. Operability-Based Approach for Process Design, Intensification, and Control: Application to High-Dimensional and Nonlinear Membrane Reactors. In *Proceedings of the FOCAPO/CPC*, 2017.
(10) Carrasco, J. C.; Lima, F. V. An Optimization-Based Operability Framework for Process Design and Intensification of Modular Natural Gas Utilization Systems. *Comput. Chem. Eng.* **2017**, *105*, 246−258.
(11) Carrasco, J. C.; Lima, F. V. Novel Operability-Based Approach for Process Design and Intensification: Application to a Membrane Reactor for Direct Methane Aromatization. *AIChE J.* **2017**, *63* (3), 975−983.
(12) Gazzaneo, V.; Carrasco, J. C.; Lima, F. V. An MILP-Based Operability Approach for Process Intensification and Design of Modular Energy Systems. *Comput.-Aided Chem. Eng.* **2018**, *44*, 2371−2376.
(13) Davis, E.; Ierapetritou, M. A Kriging Method for the Solution of Nonlinear Programs with Black-Box Functions. *AIChE J.* **2007**, *53*, 2001.
(14) Boukouvala, F.; Muzzio, F. J.; Ierapetritou, M. G. Design Space of Pharmaceutical Processes Using Data-Driven-Based Methods. *J. Pharm. Innov.* **2010**, *5*, 119.
(15) Georgakis, C. Design of Dynamic Experiments: A Data-Driven Methodology for the Optimization of Time-Varying Processes. *Ind. Eng. Chem. Res.* **2013**, *52*, 12369.
(16) Kiparissides, A.; Georgakis, C.; Mantalaris, A.; Pistikopoulos, E. N. Design of in Silico Experiments as a Tool for Nonlinear Sensitivity Analysis of Knowledge-Driven Models. *Ind. Eng. Chem. Res.* **2014**, *53*, 7517.
(17) Goyal, V.; Ierapetritou, M. G. Determination of Operability Limits Using Simplicial Approximation. *AIChE J.* **2002**, *48*, 2902.
(18) Banerjee, I.; Ierapetritou, M. G. Design Optimization under Parameter Uncertainty for General Black-Box Models. *Ind. Eng. Chem. Res.* **2002**, *41*, 6687.
(19) Li, Z.; Ierapetritou, M. G. A New Methodology for the General Multiparametric Mixed-Integer Linear Programming (MILP) Problems. *Ind. Eng. Chem. Res.* **2007**, *46*, 5141.
(20) Pistikopoulos, E. N.; Diangelakis, N. A. Towards the Integration of Process Design, Control and Scheduling: Are We Getting Closer? *Comput. Chem. Eng.* **2016**, *91*, 85.
(21) Georgakis, C.; Li, L. On the Calculation of Operability Sets of Nonlinear High-Dimensional Processes. *Ind. Eng. Chem. Res.* **2010**, *49*, 8035.
(22) Mahapatra, P.; Zitney, S. E. Dynamic Maximization of Oxygen Yield in an Elevated-Pressure Air Separation Unit Using Linear Multiple Model Predictive Control (MMPC) Framework. In *29th Annual International Pittsburgh Coal Conference 2012, PCC 2012*, 2012.
(23) Cameron, F.; Niemeyer, G.; Bequette, B. W. Extended Multiple Model Prediction with Application to Blood Glucose Regulation. *J. Process Control* **2012**, *22*, 1422.
(24) Özkan, L.; Kothare, M. V.; Georgakis, C. Model Predictive Control of Nonlinear Systems Using Piecewise Linear Models. *Comput. Chem. Eng.* **2000**, *24*, 793.
(25) Özkan, L.; Kothare, M. V.; Georgakis, C. Control of a Solution Copolymerization Reactor Using Multi-Model Predictive Control. *Chem. Eng. Sci.* **2003**, *58*, 1207.
(26) Lima, F. V.; Jia, Z.; Ierapetritou, M.; Georgakis, C. Similarities and Differences between the Concepts of Operability and Flexibility: The Steady-State Case. *AIChE J.* **2010**, *56* (3), 702−716.
(27) Lima, F. V.; Georgakis, C. Design of Output Constraints for Model-Based Non-Square Controllers Using Interval Operability. *J. Process Control* **2008**, *18*, 610−620.
(28) Lima, F. V.; Georgakis, C. Input-Output Operability of Control Systems: The Steady-State Case. *J. Process Control* **2010**, *20*, 769−776.
(29) Herceg, M.; Kvasnica, M.; Jones, C.; Morari, M. Multi-Parametric Toolbox 3.0. *Proceedings of the European Control Conference* **2013**, 502.
(30) Si, H. TetGen, a Quality Tetrahedral Mesh Generator. *AMC Trans. Math. Softw.* **2015**, *41*, 1.
(31) Rawlings, J. B.; Ekerdt, J. G. *Chemical Reactor Analysis and Design Fundamentals*; Nob Hill Publishing, Madison, WI, 2002.
(32) Carrasco, J. C.; Lima, F. V. Nonlinear Operability of a Membrane Reactor for Direct Methane Aromatization. *IFAC-PapersOnLine* **2015**, *48*, 728.
(33) EIA (U.S. Energy Information Administration). Drilling Productivity Report. https://www.eia.gov/petroleum/drilling/pdf/dpr-full.pdf (accessed Feb 28, 2019).
(34) Marcellus Shale Energy and Environment Laboratory. Well Production. http://www.mseel.org/ (accessed Feb 28, 2019).

DOI: 10.1021/acs.iecr.8b05482
Ind. Eng. Chem. Res. 2019, 58, 6069−6079